Available online at www.sciencedirect.com
SCIENCE DIRECT®
Continental Shelf Research 24 (2004) 2109–2131
CONTINENTAL SHELF RESEARCH
www.elsevier.com/locate/csr

The generation of subsurface cyclones and jets through eddy–slope interaction

L.-Y. Oey*, H.C. Zhang

Atmospheric and Oceanic Science Program, Princeton University, Sayre Hall, Princeton, NJ 08544, USA

Available online 28 September 2004

Abstract

A mechanism for the generation of subsurface cyclones and jets when a warm ring smashes onto a continental slope and shelf is proposed based on the results of a primitive-equation three-dimensional numerical model. The warm ring initially 'sits' over a slope with an adjoining shelf in a periodic channel, and its subsequent evolution is examined. The 'inviscid' response is cyclonic 'peeling-off' of the on-slope portion of the warm ring. The cyclone propagates away (to the left looking on-slope) from the warm ring, and is bottom-intensified as well as slope-trapped (cross-slope scale $\approx$ Rossby radius). The near-surface flow 'leaks' further onto the shelf while subsurface currents are blocked by the slope. The 'viscous' response consists of the formation of a bottom boundary layer (BBL) with a temporally and spatially dependent displacement thickness. The BBL 'lifts' the strong along-slope (leftward) current or jet (speed $>0.5\,\mathrm{m\,s^{-1}}$) away from the bottom. The jet, coupled with weak stratification within the BBL and convergence due to downwelling across the slope, becomes supercritical. Super-inertial disturbance in the form of a hydraulic jump or front, with strong upwelling and downwelling cell, and the jet, propagate along the slope as well as off-slope and upward into the water column. The upward propagation is halted at $z\approx z_{trap}$ when mixing smoothes out the 'jump' to an along-slope scale λ_{trap} that allows the ambient jet to bend the propagation path horizontal. At this 'matured' stage, $z_{trap}\approx -250\,\mathrm{m}$, $\lambda_{trap}\approx 50\,\mathrm{km}$, and the jet's cross-slope and vertical scales are $\approx 30\,\mathrm{km}$ and 50 m, respectively. An example that illustrates the process under a more realistic setting in the Gulf of Mexico when the Loop Current impinges upon the west Florida slope is given. The phenomenon may be relevant to the recent oil industry's measurements in the Gulf, which at times indicate jets at $z\approx -150\,\mathrm{m}$ through $-400\,\mathrm{m}$ over the slope.

Keywords: Loop current eddies; Eddy–slope interaction; Subsurface jets; Hydraulic jump; Upwelling/downwelling; Bottom boundary layer

1. Introduction

It is now well known that oceanic eddies can interact significantly with topography. Gulf

*Corresponding author. Tel: +1-609-258-5971; fax: +1-609-258-2850
E-mail address: lyo@splash.princeton.edu (L.-Y. Oey).

0278-4343/$ - see front matter © 2004 Elsevier Ltd. All rights reserved.
doi:10.1016/j.csr.2004.07.007

Stream rings have been observed to propagate onto the continental shelf/slope regions (Cheney and Richardson, 1976; Brown et al., 1986). North Brazil Current rings interact with the coast of South America as they move in a northwest direction (Richardson et al., 1994; D. Fratantoni et al., 1995). In the Gulf of Mexico, the behaviors of Loop Current Eddies (LCEs) are significantly affected by the surrounding continental slope (Lewis and Kirwan, 1985; Kirwan et al., 1988; Vukovich and Waddel, 1991; Vidal et al., 1992; Hamilton et al., 1999). Intense cyclones that often cleave the Loop Current (LC; Cochrane, 1972) maybe a result of the LC interacting with the west Florida continental slope. Model studies of eddy–slope interaction have yielded theoretical insight on the behaviors of eddy as it nears a continental slope. Earliest studies include Smith and O'Brien (1983), Smith (1986) and Smith and Bird (1989). They showed that β-dispersion causes asymmetry in the pressure distribution around an eddy leading to non-linear self-advection (see also Matsuura and Yamagata, 1982). The movement of the eddy then depends on the relative strength and orientation of planetary and topographic β. The β-dispersion also tends to obliterate lower-layer features through radiation of topographic Rossby waves, and eddies can quickly ($\sim$10 days) evolve to upper-layer features (Grimshaw et al. 1994; LaCasce, 1998). Other model studies that also examine movements of eddies in the presence of slope and/or vertical-walled boundaries include Shi and Nof (1993), Oey (1995), Zavala-Sanson et al. (1998), Nof (1999) and Sutyrin et al. (2003). For example, Nof (1999) shows that for a model warm eddy (reduced-gravity type) interacting with a western wall, eddy migration is governed by three processes. The eddy tends to move northward under the image effect, southward due to the β-induced self-advection, and northward due to the southward expulsion of mass from the eddy (the 'rocket' effect).

This paper deals with a particular aspect of a warm eddy impinging upon a continental slope: the generation of parasitic cyclones and jets. This fine-scale process has apparently not been previously addressed. The phenomenon may explain the occurrences of unusually intense sub-surface jets documented by the oil industry operating in the northern Gulf of Mexico. Fig. 1 shows an example of a LCE (the Millennium Eddy) interacting with the slope and the locations where a cyclone and a subsurface jet were observed.[1] These were observed on the convergent (left, looking onslope) side of the LCE. The jet was very strong in this case, with speeds exceeding $1\,\mathrm{m\,s^{-1}}$, occurring at depths of $z \approx -200\,\mathrm{m}$ to $-400\,\mathrm{m}$ in 1000 m of water. Fig. 2 shows the vertical speed profiles of another similar jet for a different period at a location to the southwest (91.1°W, 27.7°N) of the jet of Fig. 1. The maximum speeds in this case are about $0.5\,\mathrm{m\,s^{-1}}$, at depths of $z \approx -200\,\mathrm{m}$ in 600 m of water. In both cases, the surface currents are weak, which seems to suggest that the energy source did not originate at the surface, at least not directly. In addition to being an interesting geophysical fluid dynamical problem, the existence of subsurface cyclones and intense currents in practice requires serious attention of deepwater operators due to increased loads on offshore structures and higher risk of operations.

While the phenomenon must fundamentally be a three-dimensional one, much can be learned from the Shi and Nof's (1993; henceforth SN93) reduced-gravity model of warm eddies 'cut' by a wall (i.e. a vertical slope). They found that the fluid within the cyclonic portion of the eddy (i.e. between the outer edge of the eddy and radial position where the eddy's swirl's speed is a maximum) is advected along the wall forming a new eddy (a cyclone). The cyclone and its parent anticyclone migrate away from each other because of the image effect created by the wall. This "SN93-process" is modified if the vertical wall is replaced by a more realistic topography consisting of a continental slope and an adjoining shelf, as we schematically sketch in Fig. 3. Now only the subsurface layers of the impending warm eddy (anticyclone) 'feel' the slope while the 'wall' effect is less or non-existent for the near-surface flow. Thus the cyclone–anticyclone pair is formed in the

[1]Observations of these cyclones and jets have come solely from the oil industry, and most are proprietary. The plots shown here were kindly provided by Dr. Cort Cooper of Cheveron Inc.

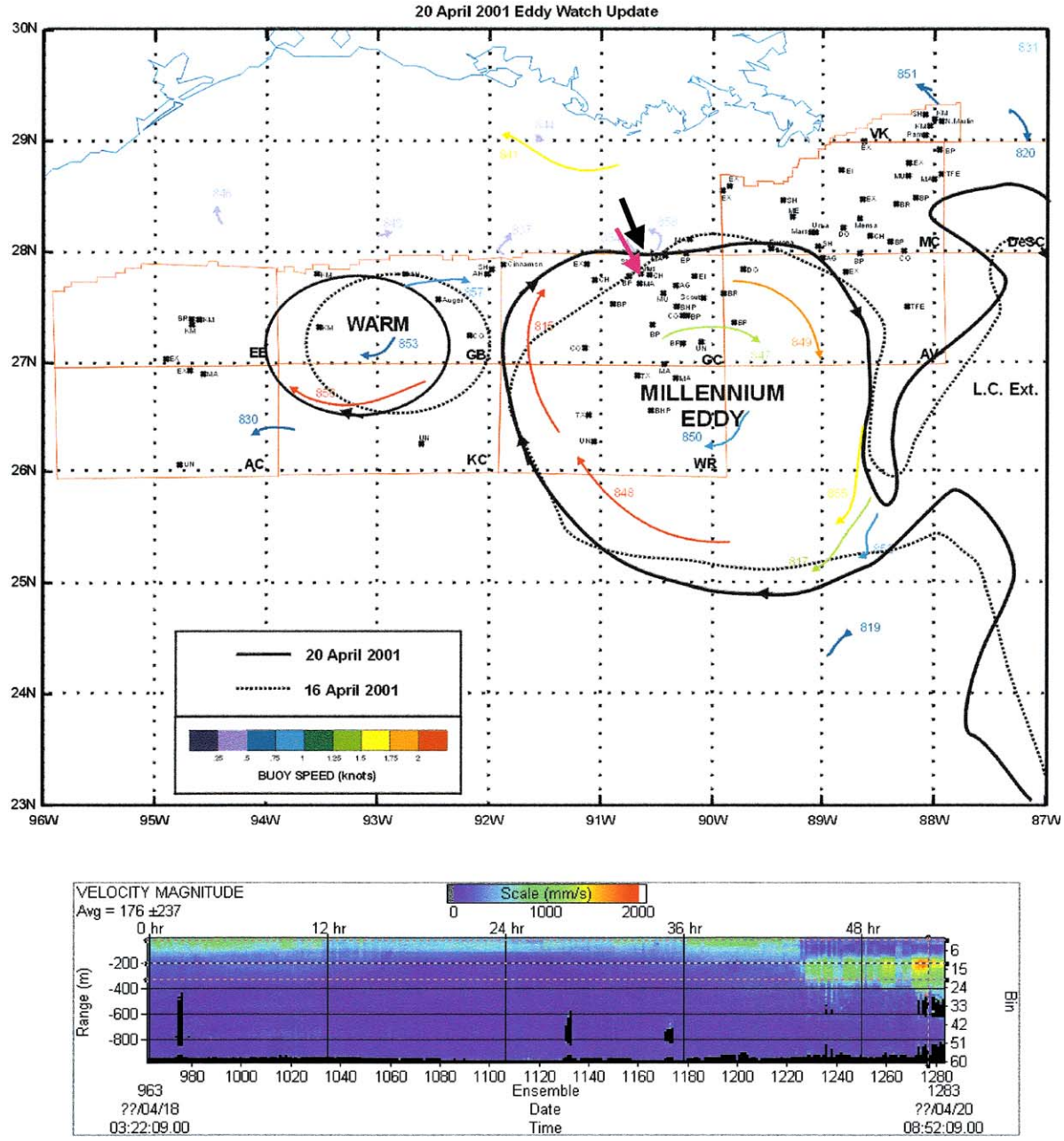

Fig. 1. Upper panel: locations of eddies and trajectories of drifters (curvy colored vectors) reported by Eddy Watch service on April 20, 2001. A small cyclonic eddy (black arrow) is located north of the Millennium Eddy close to the area where the strong current event was observed (red arrow). The local isobath is about 1000 m. Lower panel: ADCP profile in terms of speed measured at the event site. Plots courtesy of Cort Cooper of Chevron Inc.

deep, but the near-surface flow tends to continue the anticyclonic path of the parent warm eddy. The cyclone therefore tends to be strongest in the deep and diminishes near the surface, depending to some extent on the shears of the approaching warm eddy.

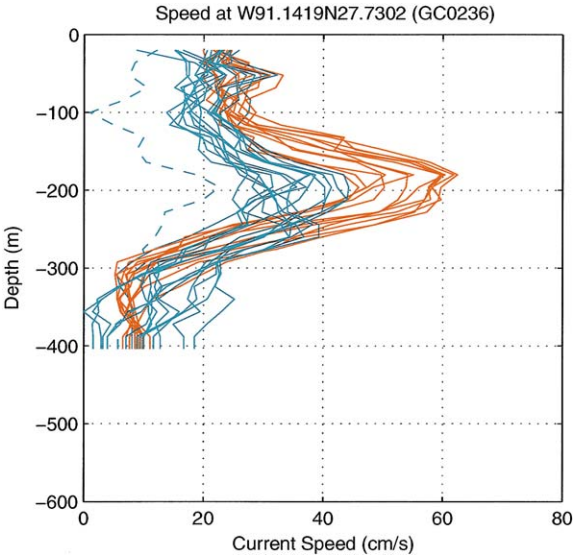

Fig. 2. Observed speed profiles at an oil industry site (91.1°W, 27.7°N; slightly to the west-southwest of the jet shown in Fig. 1) in the northern Gulf of Mexico slope, illustrating the occurrences of sub-surface jets (red solid curves) on Apr/09–10/1998. Light blue curves indicate profiles for which the maximum speed $<0.45\,\mathrm{m\,s^{-1}}$, and dashed curve indicates a profile approximately 5 days later on Apr/15, when speed at $z=-200\,\mathrm{m}$ is larger than near the surface, but weaker than earlier profiles. The local isobath is about 600 m. These curves illustrate the large temporal (and spatial) variability of the phenomenon. Plot courtesy of Chevron Inc.

The SN93-process described above is basically 'inviscid.' It can only partially explain the observations in that the cyclone and jet tend to be deep features with little near-surface expression. The presence of a viscous (turbulent) layer near the bottom can drastically change the flow picture. The convergent (i.e. on-shore) near-surface flow can now be funneled down the slope in a thin (~100 m) bottom boundary layer (BBL). The BBL can also lift the along-slope jet.

We present below two idealized model experiments that describe the inviscid SN93-process (though in three dimensions) and modifications brought about by the existence of a BBL. With the BBL, a hydraulic jump develops and propagates along-slope with the cyclone, and also propagates *upwards*. The process gives rise to intensified currents off the bottom. The paper is organized as follows. Section 2 describes the model, Section 3 the results, and Section 4 contains a discussion. Section 5 then describes and discusses an experiment that uses realistic topography and forcing in the Gulf of Mexico. Section 6 contains conclusions and Section 7 briefly discusses some future directions in shelf-edge and slope modeling.

2. Process experiments: model set up

Consider an east-west channel of length $x_L = 1000\,\mathrm{km}$ and (north–south) width $y_L = 800\,\mathrm{km}$. A tanh-profile is used for the bottom topography:

$$H = H_{deep} + \{H_{shelf} - H_{deep}\}\{1 + \tanh \times [(y - 600/50)]\}/2, \quad 0 < y < 800\,\mathrm{km}, \qquad (1)$$

where $H_{deep} = 3000\,\mathrm{m}$, $H_{shelf} = 100\,\mathrm{m}$, and $y = 0$ and $y = 800\,\mathrm{km}$ are coasts (walls). The resulting maximum topographic gradient $|\nabla h| \approx 3 \times 10^{-2}$ is quite realistic—it is a little steeper than that over the northern Gulf of Mexico, but a little less steep than that over the west-Florida slope. The Princeton Ocean Model (POM; three-dimensional primitive-equation, Bousinesq and hydrostatic, Mellor, 2002) is used with constant horizontal grid sizes, $\Delta x = \Delta y = 5\,\mathrm{km}$,[2] and with 41 equally-spaced sigma levels in the vertical. An efficient, parallelized version of POM with MPIs (Message Passing Interfaces) is used. The 2.5-level turbulence closure scheme (Mellor and Yamada, 1982) is used to model the vertical eddy viscosity and diffusivity. Shear-dependent, Smagorinsky's (1963) formulation for horizontal mixing is used with its constant $C = 0.1$ and the ratio of horizontal diffusivity to viscosity, Pr^{-1}, is set to 1/5. Oey (1996a) recommends $C \approx 0.05-0.1$, while Mellor et al. (1998) $Pr^{-1} \approx 1/5$ or smaller. The horizontal mixing is along sigma-coordinate surfaces (Mellor and Blumberg, 1985) so as to minimize spurious diffusion across BBL. Diapycnal mixing is minimized by the use of the Smagorinsky's formulation and small Pr^{-1}, and

[2] Oey (1998) suggested an empirical criterion that Δx (or Δy)/R_o should preferably be $\approx 1/3$ or less, where R_o is the baroclinic Rossby radius, $\approx 30\,\mathrm{km}$ in the present case, which gives Δx (or Δy)/$R_o \approx 1/6$.

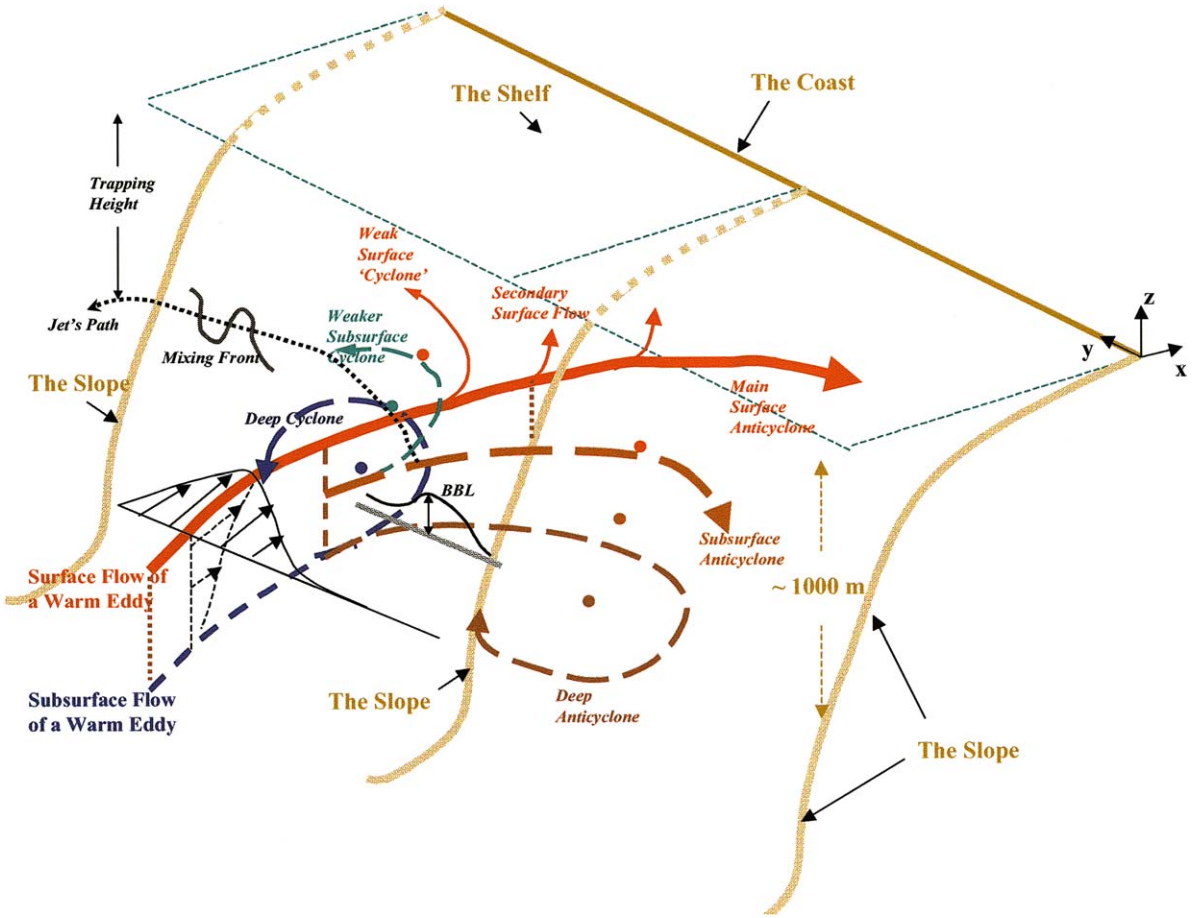

Fig. 3. A schematic sketch of deep cyclone–anticyclone pair that results when a warm eddy (thick red line) impinges upon a continental slope and shelf. The subsurface portion of the warm eddy 'feels' the slope while the surface flow intrudes further onshore and 'spills' over the shelf (thin red line). Thus the cyclone–anticyclone pair is formed in the deep (thick blue and brown dashed lines). Nearer the surface, the cyclone weakens (green dashed and thin red lines) as the flow follows the main anticyclonic path of the warm eddy (thick red line). In the presence of a BBL, a mixing front is formed and the bottom-intensified current or jet is lifted up. The front-jet system propagates along-slope, off-slope, and also *upward* as a super-inertial disturbance, until it is trapped as indicated here (dotted dark line). See text for details.

also by removing an area-averaged potential temperature field before computing the horizontal diffusion. For details please see Mellor (2002). Tests with different C and Pr^{-1} are carried out (below) to confirm the insensitivity of the modeled solutions to the above values. All fluxes are zero across the coastal boundaries ($y = 0$ and 800 km), and at the sea-surface and bottom (except for bottom drag described below). The channel is periodic in x. Both β-plane and f-plane experiments were conducted but the time scales of interest are a few days to weeks and the two sets of experiments do not differ significantly. We show the f-plane results only. The (center of) latitude is 26°N (i.e. the Gulf of Mexico) where $f = 6.393 \times 10^{-5}\,\mathrm{s}^{-1}$, corresponding to an inertial period $2\pi/f \approx 1.14$ days.

At time $t = 0$, a 'warm' eddy with depressed isotherms throughout its vertical extent (~1000 m) is placed over the slope, centered at $(x, y) = (500, 575)$ km. A balanced velocity field is obtained by fixing this initial temperature distribution and

running the model diagnostically until the maximum speed change over one time step is less than $10^{-8}\,\mathrm{m\,s^{-2}}$ (i.e. about one-tenth of the weakest Coriolis acceleration $f \times speed$, where $speed \approx 10^{-2}\,\mathrm{m\,s^{-1}}$). This was achieved in about 4–5 days. The temperature and (balanced) velocity fields at $t = 5$ days are shown in Figs. 4a and b, which are taken as the 'initial' fields from which prognostic (both density and velocity fields evolve) experiments begin. Only the temperature, T, is solved and the salinity $S = 35$ psu. The UNESCO equation of state, as adapted by Mellor (1991) is used to calculate the density, hence also the pressure gradients. The sigma-level pressure gradient error (Haney, 1991) is reduced by removing the basin-averaged density distribution (in z-only) from the time-dependent density field before evaluating the pressure gradient terms (Mellor et al., 1998). At the relatively high resolution (both vertical and horizontal) used here, 60-day test calculations using an initially level density field with perturbations (see Mellor et al., 1998) and zero forcing gives a maximum error of less than $0.1\,\mathrm{cm\,s^{-1}}$ (cf. Oey et al. 2003a).

We use a quadratic bottom drag (τ/ρ_0) formulation to specify the lower boundary conditions for (along-slope, across-slope) velocity (u,v):

$$K_M\left(\frac{\partial u}{\partial z},\frac{\partial v}{\partial z}\right) = C_d\left[u^2+v^2\right]^{1/2}(u,v), \quad z \to -H \tag{2}$$

where K_M is the vertical eddy viscosity and C_d is the drag coefficient. In experiment 1 (Expt.1), C_d is set to zero, which eliminates the BBL, while in

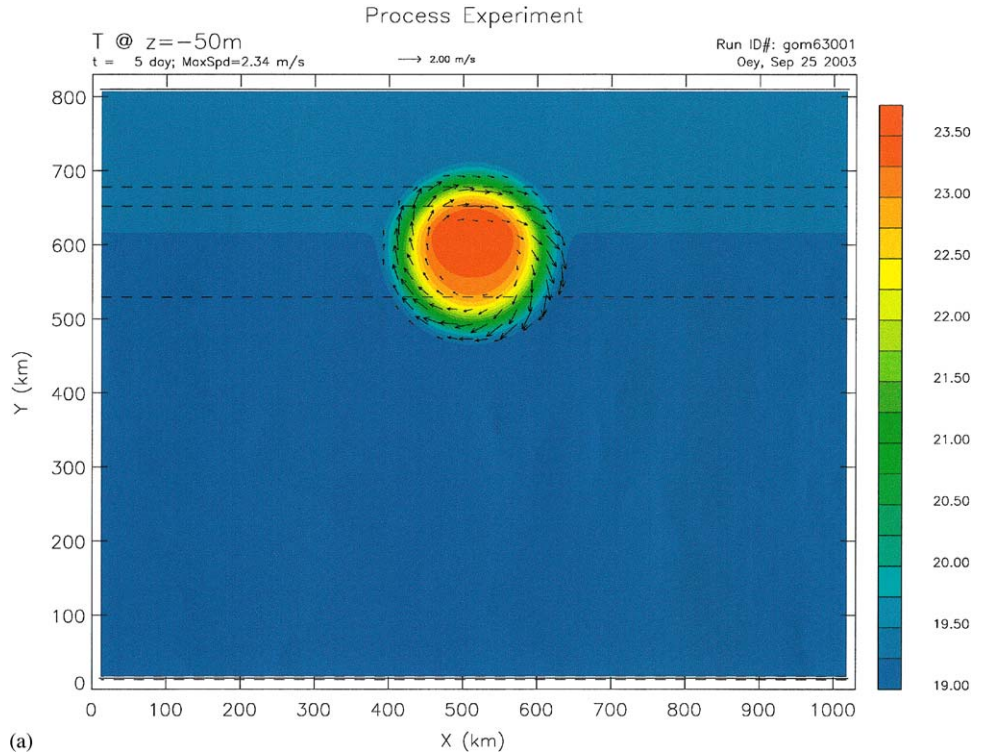

Fig 4. (a) The initial temperatures at $z = -50$ m superimposed by the geostrophically balanced velocity vectors for Process Experiments 1 and 2 in an east–west periodic channel with walls north and south. The water depth varies like a tanh-function (Eq. (1)), 3000 m near the south wall and 100 m near the north wall. The dashed lines indicate the 2900, 600 and 300 m isobaths (thus the initial warm eddy sits over the slope). (b) The initial temperature (upper panel) and geostrophically balanced along-slope velocity (lower panel) contours in an across-slope vertical section passing through the eddy centers at mid-channel ($x = 500$ km, please see Fig. 4a) for Process Experiments 1 and 2. In the velocity plot, dashed (solid) curves denote westward (eastward) currents, i.e. into (out of) the page.

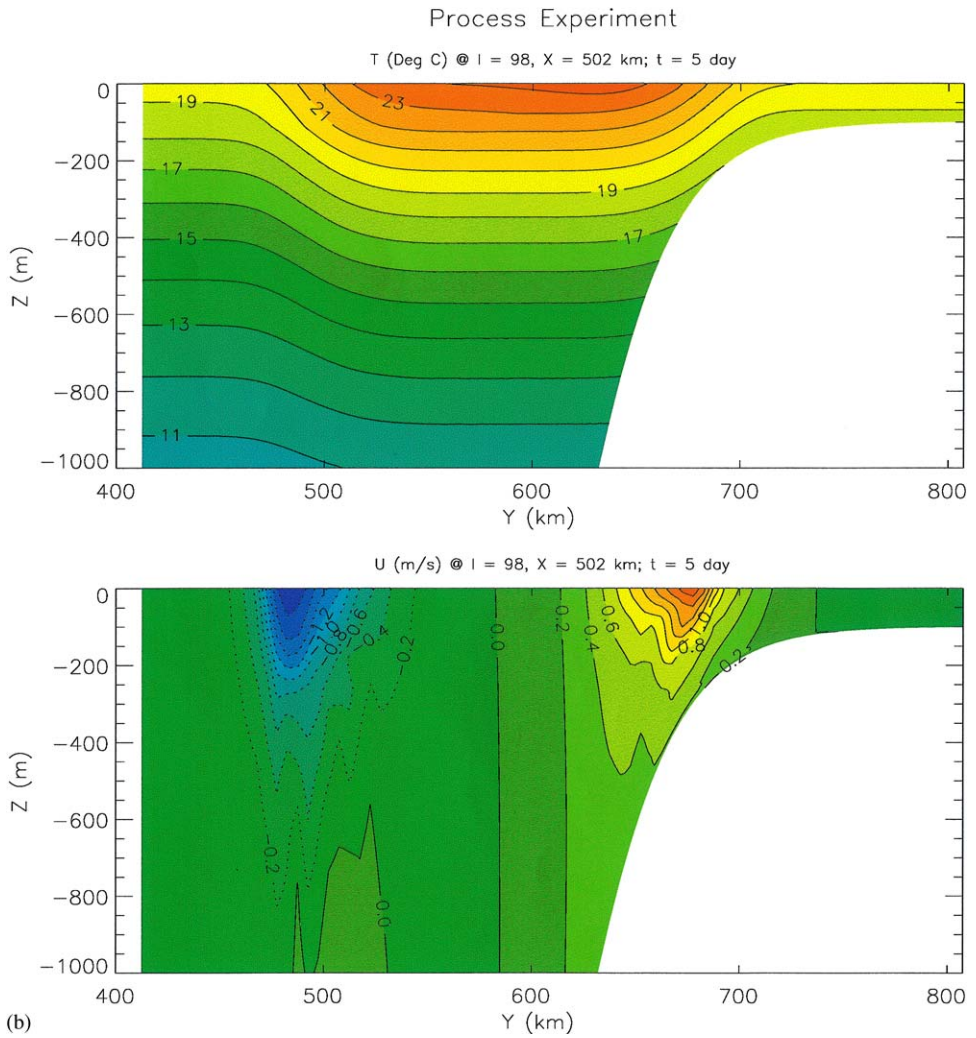

Fig 4. (*Continued*)

Expt.2, C_d is set $= 2.5 \times 10^{-3}$. Expt.1 would therefore elucidate the SN-93 process in three dimensions with more realistic slope and shelf, and Expt.2 explores the role of BBL. In the upper slope (water depths of 800 m or less), there are six or more grid points within the BBL.

3. Process experiments: results

Fig. 5 shows for Expt.1 temperature fields with velocity vectors and contours of speed superimposed, for $t = 6$ days at (a) $z = -10$ m and (b) $z = -300$ m, and also for the corresponding ones at $t = 11$ days, panels (c) and (d). At $t = 6$ days (1 day after the initial fields), a cyclone and corresponding jet are formed at $(x, y) \approx (400\,\text{km}, 660\,\text{km})$, i.e. to the left (looking on-slope) of where the warm eddy 'smashes' onto the slope. The cyclone is more developed in deeper layers (i.e. $z = -300$ m) than near the surface, in accordance with the ideas described in Fig. 3. At $t = 11$ days, the cyclone and jet propagate westward, to $x \approx 300$ km (Figs. 5c and d). Current speeds at

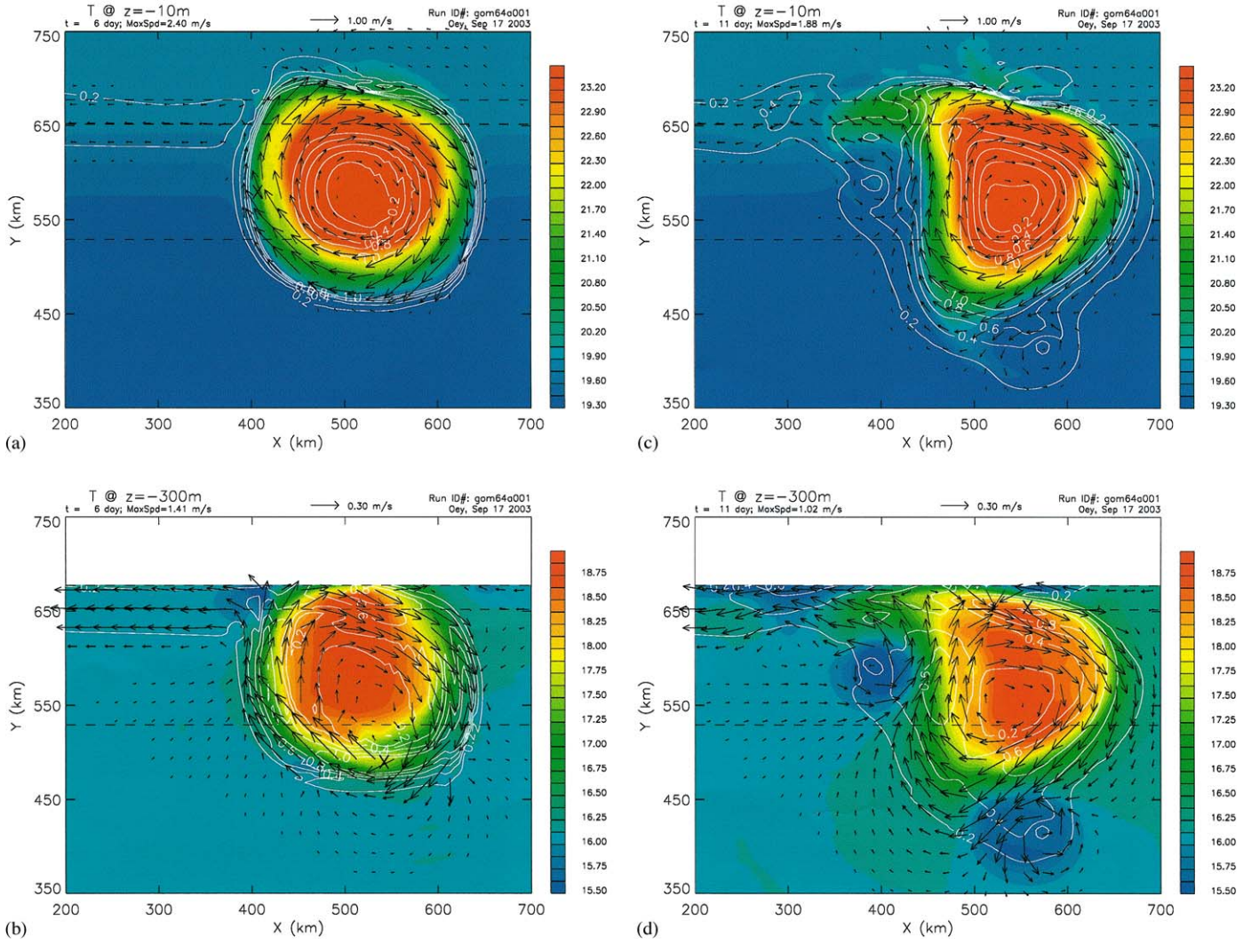

Fig. 5. Process Expt.1: temperature fields with velocity vectors and contours of speed (white; contour interval = 0.2 m s^{-1}) superimposed, for $t = 6$ days at (a) $z = -10$ m and (b) $z = -300$ m, and also for the corresponding ones at $t = 11$ days, panels (c) and (d). Note that only a partial model region focusing on the warm eddy and slope is shown.

$z = -300$ m exceed 0.6 m s^{-1}, trapped at the slope, while those near the surface are weaker ($\approx$0.3–0.4 m s^{-1}). In Figs. 5b and d there also exists a cyclone to the right of the eddy, produced by localized divergence as shelf-edge fluid is stretched; however, this cyclone is much weaker than the left-side cyclone. Note also the appearance in Fig. 5d of small-scale meanders around the warm eddy, due to instability that likely depends on the initial configuration of the eddy (e.g. Dewar et al., 1999). A study of these meanders is beyond the scope of this paper.

Fig. 6 shows *yz*-section contours of (a) speed, (b) v, (c) T and (d) w (the vertical velocity) at $t = 11$ days and $x = 312$ km (i.e. roughly passing through the slope-trapped cyclone shown in Fig. 5d). The cyclone and jet are bottom-trapped as clearly seen in the speed contours. The u-contours, not shown, are similar to the speed contours, and indicate slope-bound, bottom-intensified westward current (i.e. negative). The cross-slope currents, v, are of one order magnitude weaker than u; v is particularly weak near the bottom. Nonetheless, the v-contours indicate flow convergence over the shelfbreak. In the absence of a BBL, the convergence results in relatively weak downwelling over the shelfbreak and slope (the first and only negative w-contour in Fig. 6d is -10 m day^{-1}). Also, the isotherms (Fig. 6c) slope upward over the shelfbreak. Thus a significant portion of the convergent flow energy is expended in driving the along-slope jet trapped at the bottom.

Fig. 7 shows for the experiment with BBL (Expt.2) temperature fields with velocity vectors and contours of speed superimposed, for $t = 11$ days at (a) $z = -10$ m and (b) $z = -300$ m.

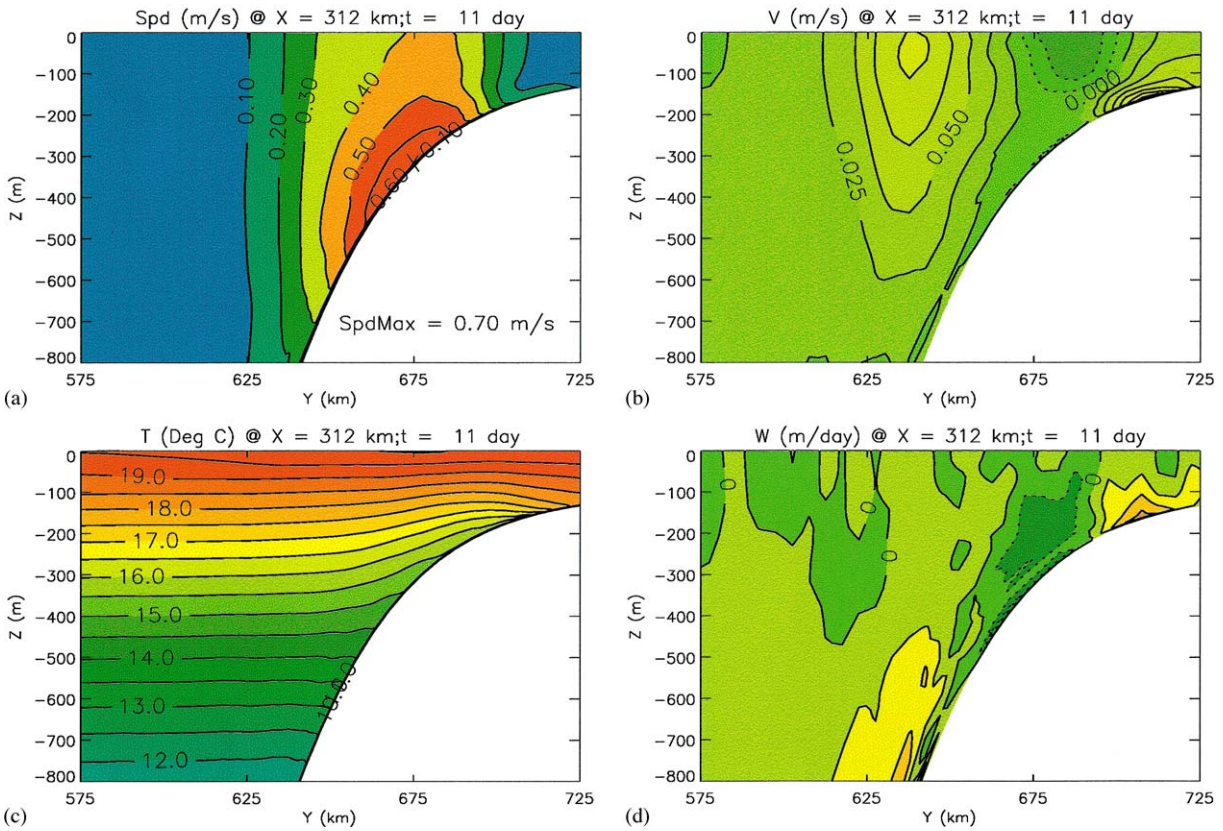

Fig. 6. Process Expt.1: *yz*-section contours of (a) speed, (b) v (the cross-slope velocity), (c) T and (d) w (the vertical velocity; contour interval = 10 m day^{-1}) at $t = 11$ days and $x = 312$ km (i.e. roughly passing through the slope-trapped cyclone shown in Fig. 5d).

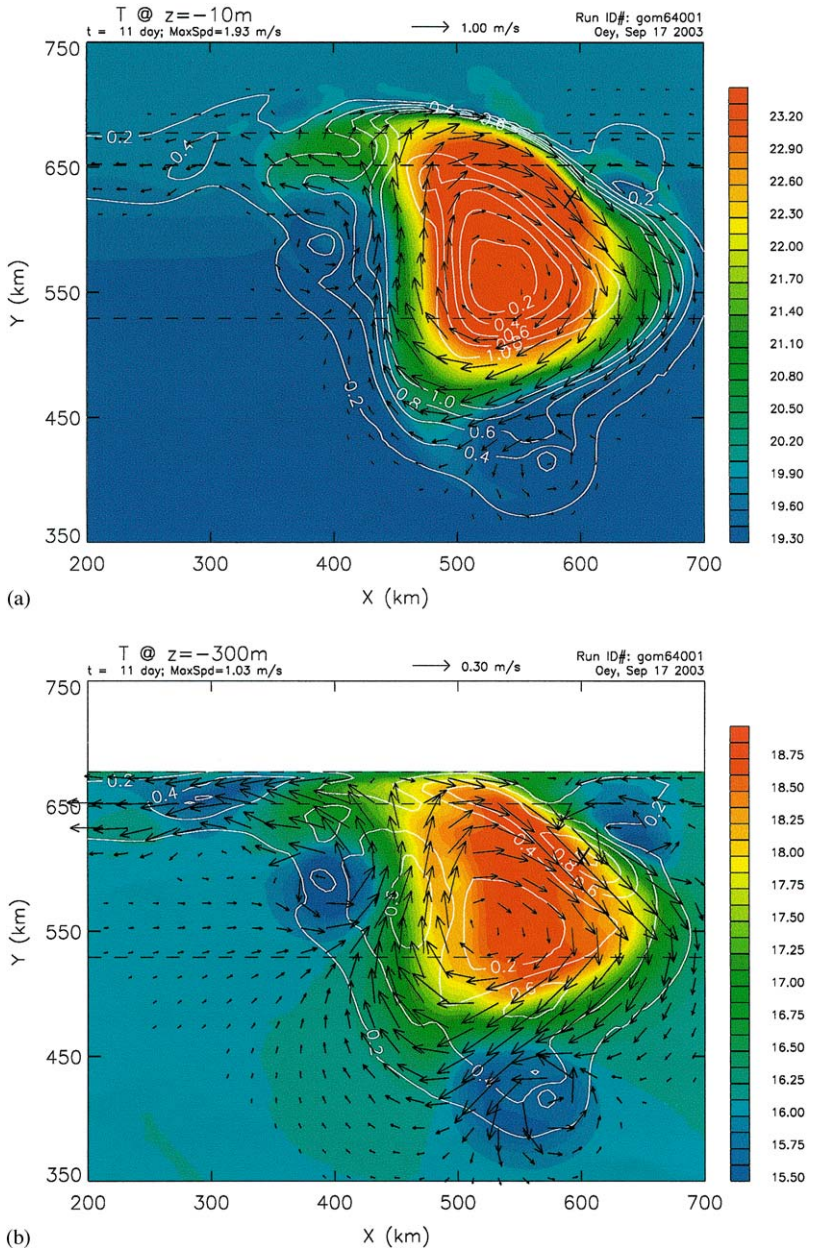

Fig. 7. Process Expt.2: temperature fields with velocity vectors and contours of speed (white; contour interval = 0.2 m s^{-1}) superimposed, for $t = 11$ days at (a) $z = -10$ m and (b) $z = -300$ m. Note that only a partial model region focusing on the warm eddy and slope is shown.

(At $t = 6$ days the plot is similar to that shown for Expt.1 in Figs. 5a and b). Comparing Figs. 7a and b with Figs. 5c and d, the subtle difference is the off-slope shift of the location of maximum velocity of the jet associated with the propagating cyclone, as can be seen in the speed contours near $(x, y) \approx (300\,\text{km}, 650\,\text{km})$. The shift can be seen clearly in Fig. 8, which shows the yz-section

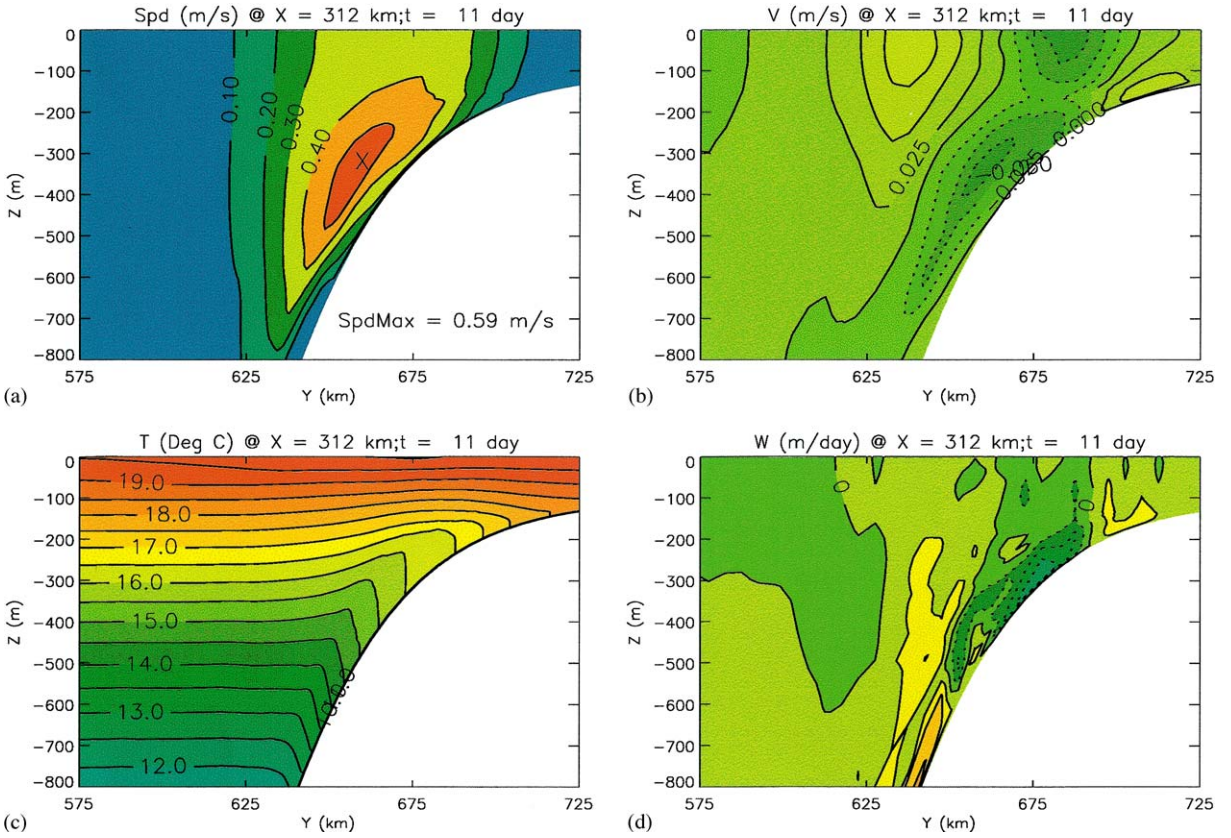

Fig. 8. Process Expt.2: *yz*-section contours of (a) speed, (b) v (the cross-slope velocity), (c) T and (d) w (the vertical velocity; contour interval = 10 m day^{-1}) at $t = 11$ days and $x = 312$ km (i.e. roughly passing through the slope-trapped cyclone shown in Fig. 5d or 7b).

contours (as in Fig. 6 for Expt.1). Comparing with Fig. 6, we see that the existence of a BBL in Expt.2 produces stronger downwelling ($w \approx -30$ m day^{-1}) and off-shore flow ($v \approx -5$ cm s^{-1}) near the bottom. The isotherms slope downward in the BBL. We also see that the region of strong along-slope westward flow ($u \approx -0.5$ m s^{-1}) is lifted off the bottom by approximately the BBL height ($\delta_{\mathrm{BBL}} = (\tau/\rho_o)^{1/2}/f$), which for the model is (from equation 2 to obtain bottom drag, with $u_{bottom} \approx 0.05-0.15$ m s^{-1}) $\approx$ 40–120 m. Before we show how these seemingly minute changes (by the BBL) can have interesting consequences to the development of subsurface jet further down-slope, we note that the downward and off-slope diversion of (a portion of) the upper-layer convergent flow into the BBL, as well as friction, generally weaken the along-slope current (compare Fig. 8a with Fig. 6a). Moreover, the cross-slope scale of region of significant current (speed) is basically determined by the 'inviscid' solution of Expt.1, and is of $O(R_o) \approx 30$ km, where R_o is the baroclinic Rossby radius.

We now examine along-slope and vertical propagation. Fig. 9 shows for Expt.1 the along-slope vertical section (*xz*-) contours of (A) temperature, (B) Froude number, $Fr = |u|/(Nh)$, where h is a height scale taken as $\approx \delta_{\mathrm{BBL}} \approx 100$ m, and (C) $N = [-(g/\rho_0)(\partial\rho/\partial z)]^{1/2}$, the Brunt–Vaisalla frequency, at $y = 652$ km from $t = 7$ through 15 days at 2-day interval. Superimposed are also contours of the three components of velocity: (A) along-slope, u, (B) cross-slope, v, and (C) vertical, w. The $y = 652$ km location corresponds approximately to the center position of the jet's core at $t = 11$ days (Fig. 8a). Fig. 10 shows the

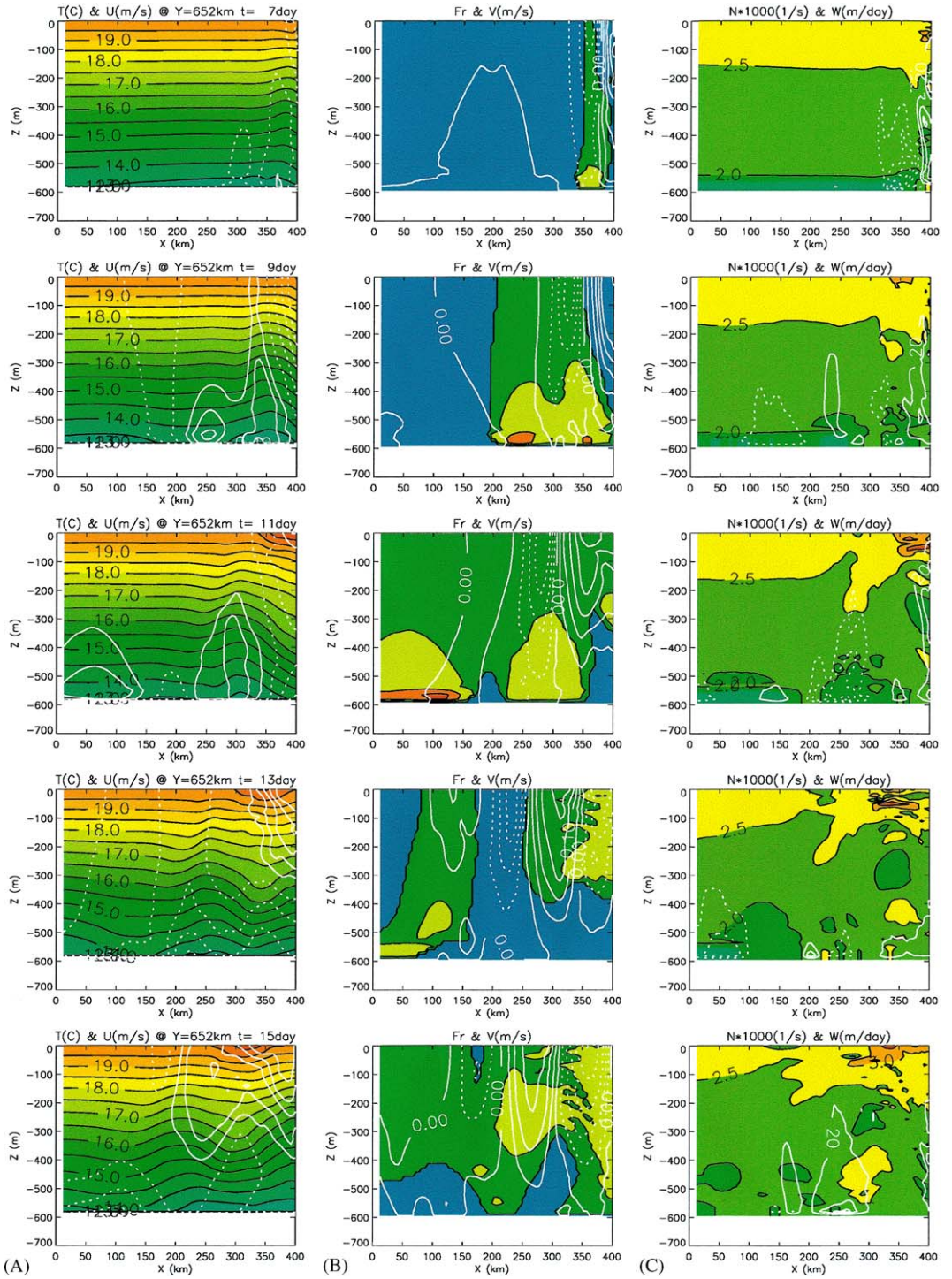
T(C) & U(m/s) @ Y=652km t= 7day
Fr & V(m/s)
N*1000(1/s) & W(m/day)
T(C) & U(m/s) @ Y=652km t= 9day
Fr & V(m/s)
N*1000(1/s) & W(m/day)
T(C) & U(m/s) @ Y=652km t= 11day
Fr & V(m/s)
N*1000(1/s) & W(m/day)
T(C) & U(m/s) @ Y=652km t= 13day
Fr & V(m/s)
N*1000(1/s) & W(m/day)
T(C) & U(m/s) @ Y=652km t= 15day
Fr & V(m/s)
N*1000(1/s) & W(m/day)
z (m)
x (km)
(A)
(B)
(C)

corresponding plots for Expt.2. In panel (A) of Fig. 10 we also superimpose a curve showing estimate of δ_{BBL} computed from $(\tau/\rho_0)^{1/2}/f$. In both figures, the right-edge of the plot (at $x = 400$ km) corresponds approximately to the position where the cyclone and jet were first formed (cf. Figs. 5a and b) at $t = 6$ days. This formation can be seen at $t = 7$ days as (slight) up-doming of isotherms in (A), offshore (negative) and onshore v centered around $x = 380$ km in (B), and downwelling and upwelling about the center in (C). Downwelling occurs to the left of the cyclone's center. At this time, there is only a weak (≈ 0.1–$0.2\,\mathrm{m\,s^{-1}}$) westward current along the slope, mostly near the cyclone-formation region. For Expt.2, δ_{BBL} thickens near this region also. Near the bottom, values of N are smaller for Expt.2 because of mixing in the BBL.

At $t = 9$ days, westward flow strengthens. It is most intense at the bottom for Expt.1 and just outside the BBL for Expt.2. In Expt.2, the 14°C isotherm intersects the bottom at $x \approx 300$ km due to mixing, while in Expt.1 the isotherms are 'inviscid' expressions of the cyclone. A near-bottom mixing 'front' (a hydraulic jump) of height $\approx \delta_{BBL}$ is formed in Expt.2. This mixing and frontal-formation process occurs rapidly (several hours), and coincides with the rapid variation of the bottom drag (i.e. also the δ_{BBL}). The Froude number Fr becomes large (≈ 1) near the front where δ_{BBL} also peaks. The region of low N (<2) near the bottom thickens as mixing intensifies. The contrast between Expt.2 and Expt.1 is clear; the latter maintains its stratification near the bottom, i.e. N remains quite large and Fr small.

From $t = 11-15$ days, the mixing front and region of large Fr (i.e. the jet region) propagate *upward* as well as along the slope. The front and jet are also advected offshore by the downstream portion of the cyclone. The w-field at $t = 11$days begins to show intense upwelling ($+20\,\mathrm{m\,day^{-1}}$) and downwelling ($-40\,\mathrm{m\,day^{-1}}$) cell typical of frontal structure (Wang, 1993) at $x \approx 280$ km. These strengthen further at $t = 13$ and 15 days (especially upwelling, up to $+60\,\mathrm{m\,day^{-1}}$). At $t = 15$ days, the jet maintains an intense speed of $0.45\,\mathrm{m\,s^{-1}}$ at $z \approx -250$ m. Note that a weak anticyclone is formed below the front (and the jet). The isotherms exhibit the characteristic of a 'U' shape capped by a dome inside of which the fluid is well-mixed. The mixing has smoothed the hydraulic jump, and its horizontal scale is now 40–50 km. Hamilton et al. (2002) have noted such small-scale features in hydrographic measurements of the upper slope of the north central Gulf of Mexico.

4. Process experiments: discussions

Within a few days of the warm eddy's impact upon the slope, the jet (with speeds $\approx 0.5\,\mathrm{m\,s^{-1}}$) occurs off the slope at subsurface $z \approx -400$ to -200 m in water depths of about 600 m–1000 m (Fig. 10). The time scale of its occurrence is less than 1 day (at a fixed location where the event passes). These characteristics are due to the existence of a BBL formed due to bottom intensification of current when the warm eddy smashes onto the slope. Bottom currents produce mixing. The time scale t_{mix} of mixing and frontal formation is short, it is $\approx (h_{mix})^2/K_M$, where h_{mix} is a mixing length scale and K_M from the model is ≈ 0.01–$0.04\,\mathrm{m\,s^{-2}}$ inside the BBL under the jet. Take h_{mix} to be some fraction of δ_{BBL}, say the displacement thickness $\delta_1 \approx \delta_{BBL}/3$ for a boundary layer on a flat plate (Schlichting, 1968), t_{mix} is then ≈ 12 h. One may think of the external ('inviscid') streamlines as being 'deflected' by an instantaneous appearance of a bump or seamount caused by the BBL, then becoming supercritical and forming a hydraulic jump as described

Fig. 9. Process Expt.1: the along-slope vertical section (xz-) contours (in black) of (A) temperature, (B) Froude number, Fr (contour min/max = 0.2/1.4, interval = 0.4) and (C) Brunt-Vaisalla frequency, $N \times 10^3$ (contour min = 0.5, interval = 0.5), at $y = 652$ km from $t = 7$ through 15 day at 2-day interval. Superimposed are also contours (in white) of the three components of velocity: (A) along-slope, u (solid contours -0.4, -0.45, -0.5, etc; dotted contours: -0.3, -0.2, -0.1, etc.), (B) cross-slope, v (contour min = -0.25, interval = 0.05 up to max = 0.25, then increment = 0.25, and (C) vertical, w (contour interval = $20\,\mathrm{m\,day^{-1}}$ and the zero-contour is omitted). Negative contours are dotted in (B) and (C).

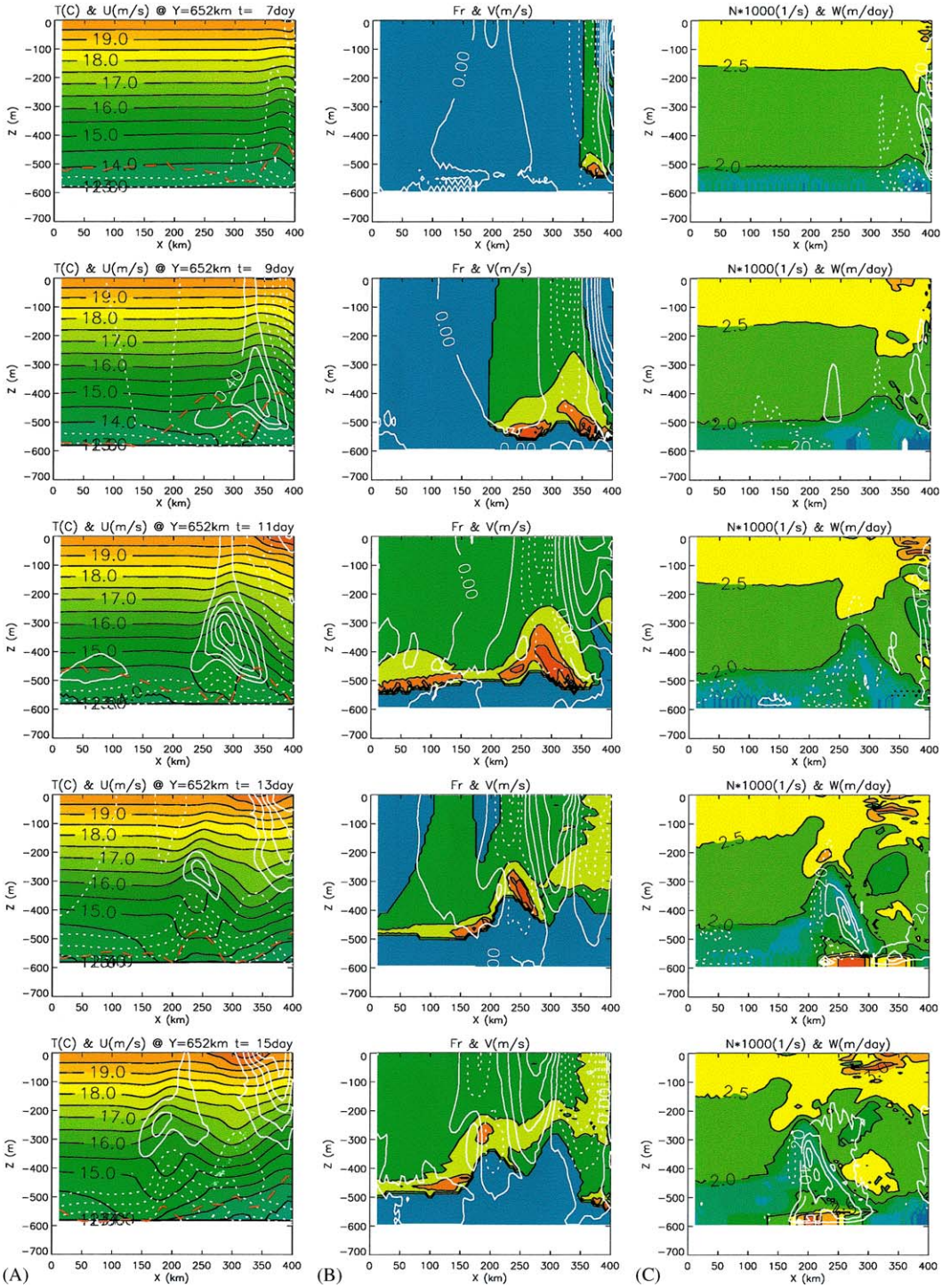
T(C) & U(m/s) @ Y=652km t= 7day
Fr & V(m/s)
N*1000(1/s) & W(m/day)
T(C) & U(m/s) @ Y=652km t= 9day
Fr & V(m/s)
N*1000(1/s) & W(m/day)
T(C) & U(m/s) @ Y=652km t= 11day
Fr & V(m/s)
N*1000(1/s) & W(m/day)
T(C) & U(m/s) @ Y=652km t= 13day
Fr & V(m/s)
N*1000(1/s) & W(m/day)
T(C) & U(m/s) @ Y=652km t= 15day
Fr & V(m/s)
N*1000(1/s) & W(m/day)
z (m)
x (km)
(A)
(B)
(C)

previously. The short time scale of t_{mix} allows the excitation of super-inertial disturbance (the hydraulic jump and jet) that propagates *upward* (Gill, 1982).

Note that the disturbance is finite-amplitude—it continuously modifies its environment. It is trapped at $z_{trap} \approx -250$ m and at $t \approx 13-15$ days when a sharp vertical gradient in N may be seen in Fig. 10c. However, at the present 'hydrostatic rotating range' (hydrostatic, but time scale of disturbance $< 2\pi/f \approx 1.14$ days), N-variation plays little role in trapping the disturbance. On the other hand, Fig. 10 shows clearly that the disturbance that begins as a hydraulic jump (or front) at $t = 7$–9 days 'smoothes out' as it propagates upward. At $t = 13-15$ days, the spatial scale or 'wave-length' λ_{trap} of the disturbance lengthens, $\lambda_{trap} \approx 50$ km. This scale may be compared with that derived from ray-tracing analysis, which gives $\lambda_{ray} = U.2\pi/f$ as the wavelength when vertically propagating ray is 'turned back,' where U is the ambient flow speed (Gill, 1982). Take $U \approx 0.5\,\mathrm{m\,s^{-1}}$ (from Fig. 10), we obtain $\lambda_{ray} \approx 50\,\mathrm{km} \approx \lambda_{trap}$. The ray analysis is not strictly valid in the present case (in which the U and N do not vary 'slowly'). Nonetheless, z_{trap} may be interpreted as the height at which the wavelength of the vertically propagating mixing front has smoothed out sufficiently to allow self-trapping by its own current.

The along-slope progression of cyclone and associated upward propagation of the jump and jet system can also be illustrated by following the tracer that initially is embedded in the BBL. Fig. 11 shows snapshots of the tracer contours (white) superimposed on the temperature fields at $t = 6$, 10, 14 and 18 days at the same along-slope vertical section ($y = 652$ km) as Fig. 10. Within a few days, the tracer is swept downstream (i.e. to the left). The resulting convergence produces a front (the hydraulic jump) that lifts the tracer out of the BBL. The tracer front subsequently 'breaks' around $t \approx 12-13$ days and intense mixing ensues downstream. The pictures at t=14 and 18 days show continued downstream and upward progression of the front. The tracer is 'scooped' up to a height of $z \approx -200$ m from the BBL in about 10 days, or an ascent rate of about $30\,\mathrm{m\,day^{-1}}$. The cyclone, jump and jet system therefore provides an efficient means by which deep dormant fluids are brought up to more active layers nearer the surface.

4.1. Additional experiments

Additional experiments were conducted to verify the above findings for Expt.2 when (a) horizontal grid resolution is doubled, $\Delta x = \Delta y = 2.5$ km instead of 5 km; (b) number of vertical sigma-levels is doubled, 81 instead of 41; (c) the bottom drag coefficient is doubled, $C_d = 5 \times 10^{-3}$; (d) C_d is variable given by matching the velocity near the bottom to a logarithmic profile (a default in *POM*, see Mellor, 2002):

$$C_d = \mathrm{MAX}\left[\frac{\kappa^2}{\left[\ln\{z_b/z_o\}\right]^2}, 0.0025\right], \tag{3}$$

where $\kappa = 0.4$ is the von Karman constant, $z_0 = 0.01$ m is the roughness parameter, and z_b is the z-value of the grid cell closest to the bottom; (e) the Smagorinsky's constant ($C = 0.1$ for Expt.2) is changed, = 0.05 (smaller) and also = 0.125 (larger); (f) the Coriolis parameter f is doubled so that $2\pi/f \approx 13.6$ h (instead of 27.36 h for Expt.2); and (g) the ratio of horizontal diffusivity to viscosity, Pr^{-1}, is reduced to 1/10 (instead of 1/5). Eq. (3) gives $C_d = 2.5 \times 10^{-3}$ for water depth $H > 2300$ m,

Fig. 10. Process Expt.2: the along-slope vertical section (xz-) contours (in black) of (A) temperature, (B) Froude number, Fr (contour min/max = 0.2/1.4, interval = 0.4) and (C) Brunt–Vaisalla frequency, $N \times 10^3$ (contour min = 0.5, interval = 0.5), at $y = 652$ km from $t = 7$ through 15 day at 2-day interval. Superimposed are also contours (in white) of the three components of velocity: (A) along-slope, u (solid contours −0.4, −0.45, −0.5, etc; dotted contours: −0.3, −0.2, −0.1, etc.), (B) cross-slope, v (contour min = −0.25, interval = 0.05 up to max = 0.25, then increment = 0.25, and (C) vertical, w (contour interval = $20\,\mathrm{m\,day^{-1}}$ and the zero-contour is omitted). In (A) we also superimpose a curve (red dash) showing estimate of δ_{BBL} computed from $(\tau/\rho_0)^{1/2}/f$. Negative contours are dotted in (B) and (C).

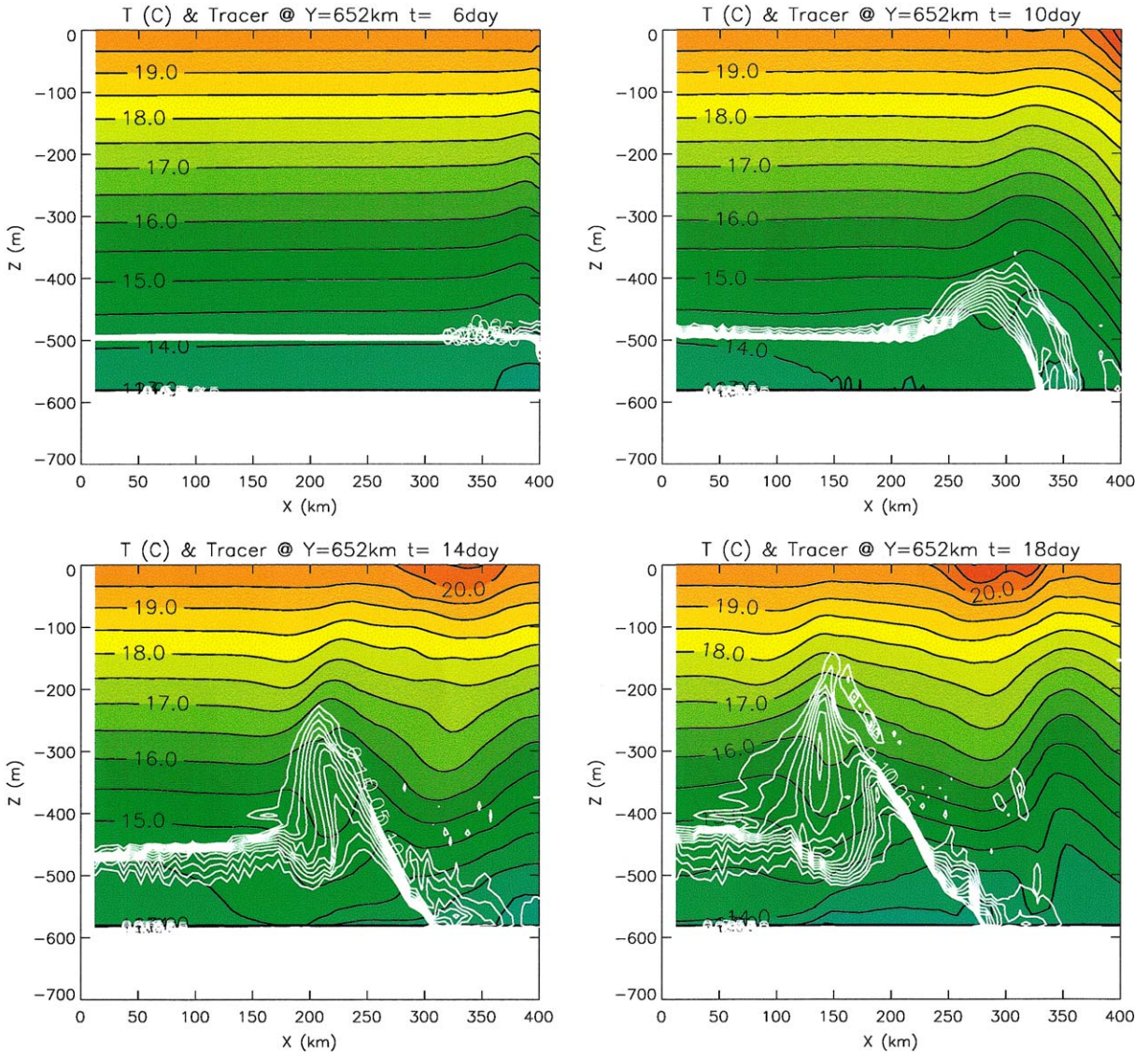

Fig. 11. Process Expt.2: snapshots of the tracer contours (white) superimposed on the temperature fields at $t = 6$, 10, 14 and 18 days at the same along-slope vertical section ($y = 652$ km) as Fig. 10. Initially (i.e. at $t = 6$ days), tracer = 1 inside the BBL (i.e. $z < -500$ m) and = 0 elsewhere. Tracer contours are 0.05–0.95 at an interval = 0.05.

$C_d \approx 3.15 \times 10^{-3}$ for $H = 1000$ m and $C_d \approx 4.6 \times 10^{-3}$ for $H = 300$ m. The corresponding experiments will be referred to as Expt.2a, Expt.2b, etc.

In general, the solutions and corresponding physics described previously are insensitive to changes in grid resolution, bottom drag, Smagorinsky's constant and Pr^{-1}. Expt.2e with decreased (increased) $C = 0.05$ (= 0.125) increases (decreases) the maximum jet's speed by about 6%. As expected, the smaller C also gives a noisier field. The solution is virtually unchanged when Pr^{-1} is decreased (not shown), which suggests that diapycnal mixing is insignificant. Fig. 12 shows cross-slope sectional contours of speed for (a) Expt.2, (b) Expt.2a, (c) Expt.2c and (d) Expt.2b at $x = 192$ km for (a), (c) and (d) and $x = 186$ km for

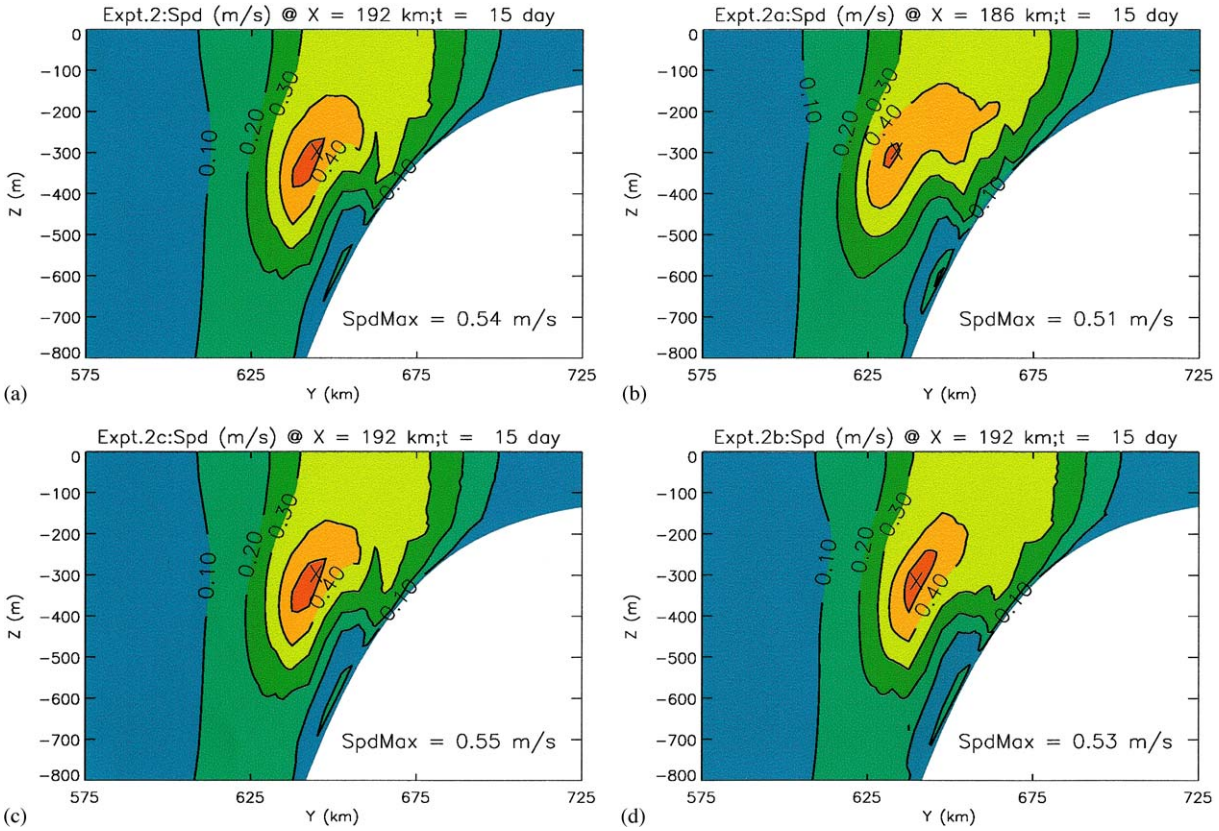

Fig. 12. Cross-slope sectional contours of speed for (a) Expt.2, (b) Expt.2a (doubled horizontal resolution), (c) Expt.2c (changed bottom drag coefficient) and (d) Expt.2b (doubled vertical resolution) at $x = 192$ km for (a), (c) and (d) and $x = 186$ km for (b), at $t = 15$ days. The x-position in each panel is chosen so the section passes through region of maximum speed at that time; cf. Fig. 10.

(b), at $t = 15$ days (the x-position is chosen so the section passes through region of maximum speed at that time; cf. Fig. 10). Changing the C_d (provided that it remains finite; Fig. 12c) gives insignificant change to the location and intensity of the jet (the variable C_d case, Expt.2d, gives almost identical plot as for Expt.2 in Fig. 12a), so does the doubling of the vertical resolution (Fig. 12d). Doubling the horizontal resolution (Fig. 12b) weakens the jet slightly. Stronger cross-slope motions (i.e. meanders) ensue however (not shown), which result in the maximum jet being shifted slightly offshore and further downstream, by about 10 km. These differences are minor however, and the basic underlying physics (BBL, off-slope and upward propagation of jet, etc.) remain. The most dramatic change occurs for Expt.2f when the Coriolis parameter is doubled, for which upward propagation of jet ceases as the near-bottom motions become sub-inertial (not shown).

5. A more realistic experiment

To confirm the above cyclone and jet-generation mechanism under a more realistic model setting, we conducted a series of hindcast experiments (from 1992 through 1999) of the Loop Current and Loop Current eddies, and examined cases when they impinge onto the slopes and shelves of the eastern and northern Gulf of Mexico. The findings

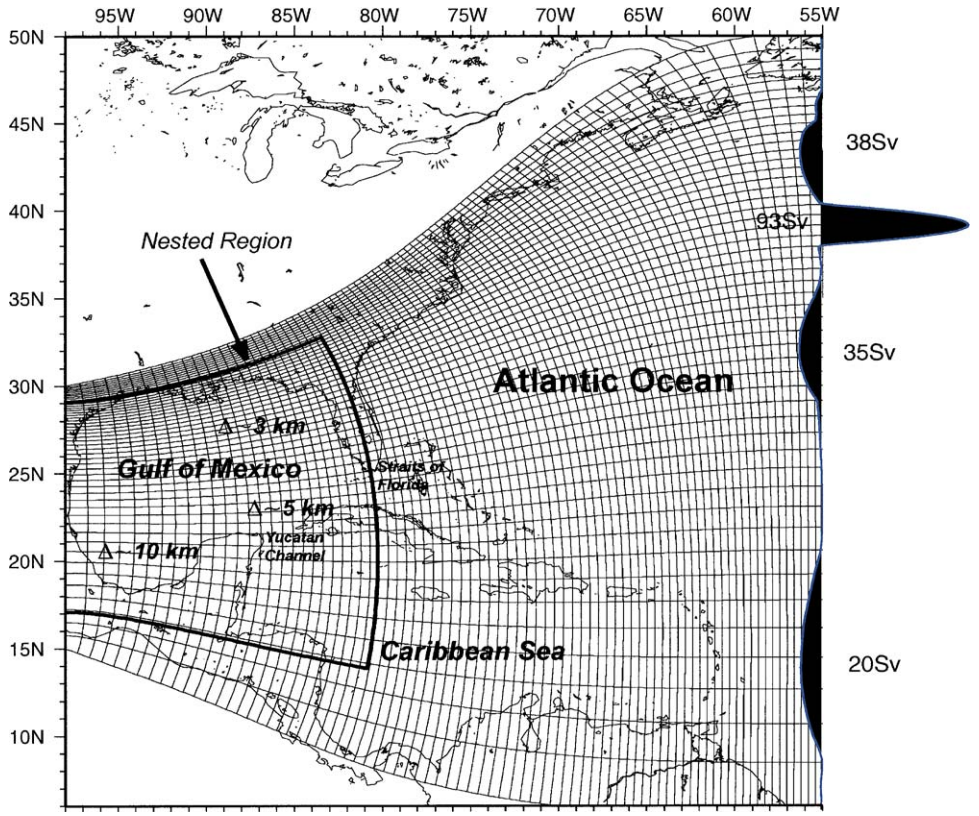

Fig. 13. The Oey et al.'s (2003a) northwest Atlantic Ocean model domain and the nested, doubled-resolution Gulf of Mexico region where calculations described herein are conducted. The "parent" grid lines are shown at every seventh grid point, and the approximate distribution of doubled-resolution grid sizes in the nested Gulf is indicated. There are 25 sigma levels in the vertical, with vertical grid sizes less than 5 m near the surface over the deepest region of the Gulf (~3500 m). Time-independent inflow and outflow transport profile, as a function of latitude (y), is specified across the 55°W as shown.

will be detailed in Oey et al. (2003c), and an example for a case without satellite data assimilation is described here.

The basic model is that of Oey et al. (2003a; hereinafter referred to as OLS).[3] The model employs actual (realistic) bathymetry interpolated from GTOPO-30 (30-second resolution data from a combination of satellite and soundings provided by the US Geological Survey), and further edited on the shelves with NOS (National Ocean Survey) charts. Time-independent transports (from Schmitz, 1996) are specified at the model's only open boundary at 55°W (Fig. 13). These transports determine the two-dimensional depth-integrated velocities and approximate the large-scale transports (windcurl + thermohaline) through 55°W. The open-boundary conditions are a combination of these transport specifications along with radiation and advection as detailed in Oey and Chen (1992a). For example, the temperature (T) and salinity (S) fields are advected using one-sided difference scheme when flows are eastward (that is, outflow), and are prescribed from monthly T and S from the Generalized Digital Environmental Model (GDEM) climatology (Teague et al., 1990) when flows are westward. These open-boundary specifications also set the

[3]The model is the orthogonal curvilinear grid, sigma-coordinate Princeton Ocean Model (POM). Besides OLS, other references include Oey and Lee (2002), Ezer et al. (2003), Oey et al. (2003b), and Wang et al. (2003).

baroclinic structure, which in the present case is largely geostrophic through the thermal-wind balance. All fluxes are zero across closed boundaries. At the sea-surface, climatological heat and salt fluxes are used and six-hourly wind stresses for the period 1992–1999 from the European Center for Medium-range Weather Forecast are specified. To resolve the subsurface cyclones and jets, OLS' horizontal grid resolution in the Gulf of Mexico is doubled by nesting the Gulf within the OLS' domain, as shown in Fig. 13. The nesting results in $\Delta x \approx \Delta y \approx 2$–$5$ km in the eastern and northern Gulf. The nesting follows that given in Oey and Chen (1992b) and Oey (1996a, b), except that one-way interaction only, from coarse to fine, is used. Volume, heat and salt fluxes are thus specified from the coarse grid to the fine grid. The baroclinic velocity field along the nested boundary is allowed to evolve by applying the Sommerfeld radiation condition (Oey and Chen, 1992b) together with Kurihara and Bender's (1980) relaxation scheme. Twenty-five sigma levels are used in the vertical. The sigma-level pressure gradient error (Haney, 1991) is again reduced by removing the basin-averaged density distribution (in z-only) from the time-dependent density field before evaluating the pressure gradient terms (Mellor et al., 1998). OLS show that the maximum error $\approx 0.15\,\mathrm{cm\,s^{-1}}$, which is relatively small in comparison to, say, the Loop Current speeds $\approx 1\,\mathrm{m\,s^{-1}}$. The Smagorinsky's (1963) mixing coefficient is set to 0.1, and the ratio of (horizontal) diffusivity to viscosity, Pr^{-1}, is 0.2, same values as for Expt.2. The initial conditions are climatological T/S with the corresponding geostrophically balanced velocity fields. The integration was carried out for eight years, from 1992 through 1999.

We show here an example of formation of subsurface cyclone and jet over the west Florida slope. Here the Loop Current strikes the slope and turns sharply southward. Fig. 14 shows contours of sea-surface height on $t_1 = 98/09/01$ (left panels) and 11 days later on $t_2 = 09/12$ (right panels), red is high $\geqslant 0.6$ m and blue is low $\leqslant -0.6$ m. Superimposed are trajectories colored with values of relative vorticity (non-dimensionalized by f), red is anticyclonic $\leqslant -0.4$ and blue is cyclonic $\geqslant 0.4$ at $z = -20$ m (upper panels) and $z = -400$ m (lower panels). The (model) Loop Current is seen on t_1 to extend northwestward to south of Mississippi delta. It then swings east (after shedding a small anticyclone "W") and on t_2 strikes the west Florida slope. Similar to the findings of process Expt 2, we find the subsurface intensification of cyclone, as well as the generation and propagation of mixing front and jet along the position indicated by the thick-dashed arrow. (The appearances of cyclonic meanders along the northern and eastern portions of the LC are often seen in satellite data, e.g. Vukovich and Maul, 1985; P. Fratantoni et al., 1998). The trapping height $z_{trap} \approx -300$ m in this case, and the jet propagates northwestward along the slope, trapped at this height. Fig. 15 shows a picture of the subsurface jet: vectors at $z = -50$ m (black) and -300 m (colored) on Sep/05/1998. The large black and red vectors near the south/southwestern portion of the figure indicate the northern edge of the model Loop Current. Against the slope, a cyclone and north/northwestward jet (red vectors) with speeds $\approx 0.5\,\mathrm{m\,s^{-1}}$ can be seen. Near-surface currents above the jet are weak (short black vectors).

6. Conclusions

We show that subsurface cyclones and jets can be generated on the convergent side of a warm eddy smashing onto a slope with an adjoining shelf. The cyclones and jets are bottom-intensified since the convergent flow is blocked by the slope at depth. The BBL plays an important role in creating a temporally and spatially dependent displacement thickness that deflects the jet which, together with low stratification in the BBL, results in the formation of a mixing front or hydraulic jump. The response is super-inertial and the 'jump' and jet system propagates along-slope, off-slope and also *upward*. The upward propagation is stopped (and the jet is 'trapped') at a height z_{trap} when the scale of the disturbance lengthens (i.e. the 'jump' spreads), $= \lambda_{trap} \approx U.2\pi/f$, where U is the jet's speed. Typical values of $z_{trap} \approx -250$ to -300 m. The proposed process is summarized schematically in Fig. 3. The upward propagation and trapping are important model findings that

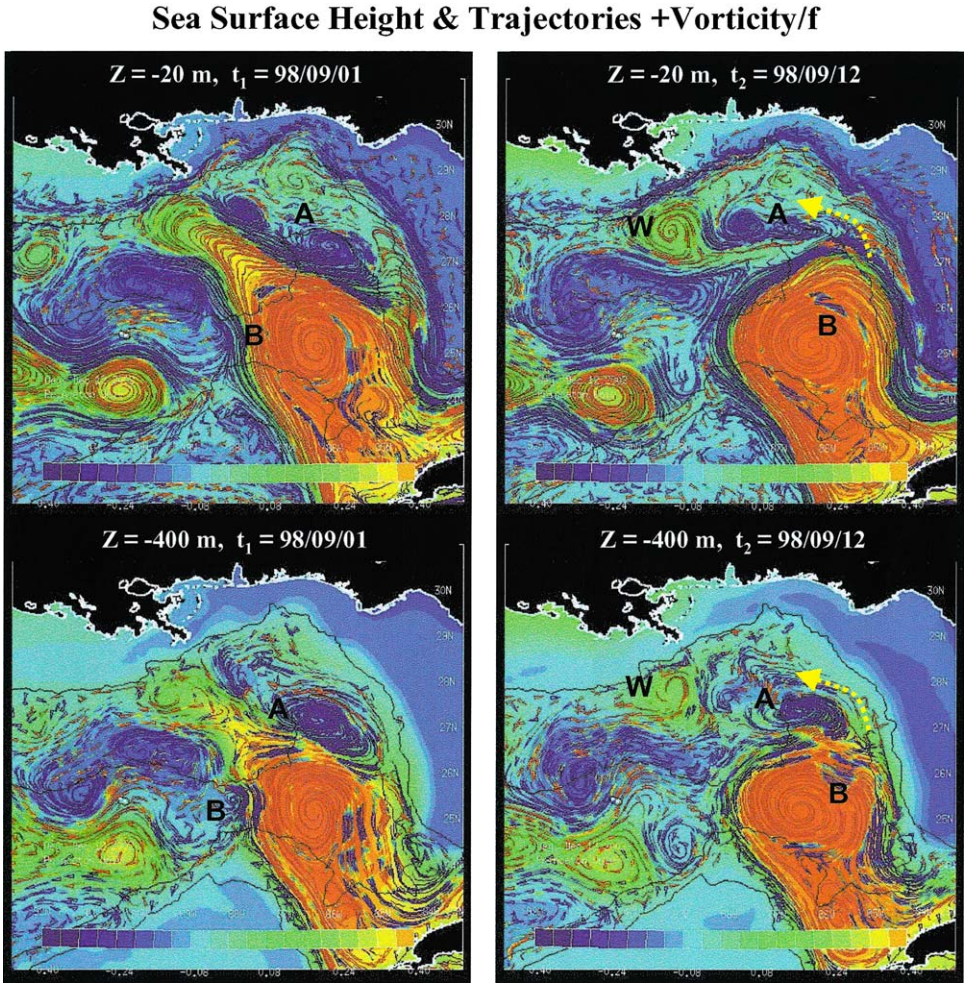

Fig. 14. Model of the Loop Current in the Gulf of Mexico: contours of sea-surface height on $t_1 = 98/09/01$ (left panels) and $t_2 = 09/12$ (right panels), red is high $\geqslant 0.6$ m and blue is low $\leqslant -0.6$ m. Superimposed are 5-day trajectories centered on respective dates and colored with values of relative vorticity non-dimensionalized by the Coriolis parameter f, red is anticyclonic $\leqslant -0.4$ and blue is cyclonic $\geqslant 0.4$ at $z = -20$ m (upper panels) and $z = -400$ m (lower panels). Labels A and B are cyclones and W is anticyclone. Yellow dashed arrow indicates location where subsurface jets are found. Dark contours show the 200 and 3000 m isobaths.

may explain why ADCP measurements by the industry often find intermittent jets at this level (z_{trap}) over the slope.

7. Future challenges

As exemplified by the above results, shelf-edge and slope are regions where larger-scale, slower-time open-ocean currents (warm eddy) coexist with finer-scale, fast-time coastal or topographic physics (BBL mixing and trapped current; see also Davies and Xing, 2000). The coexistence or overlapping of scales requires a model that resolves both processes; this makes shelf-edge and slope problems particularly challenging. Such a model is viable with more powerful yet affordable computers (clusters) and more efficient codes

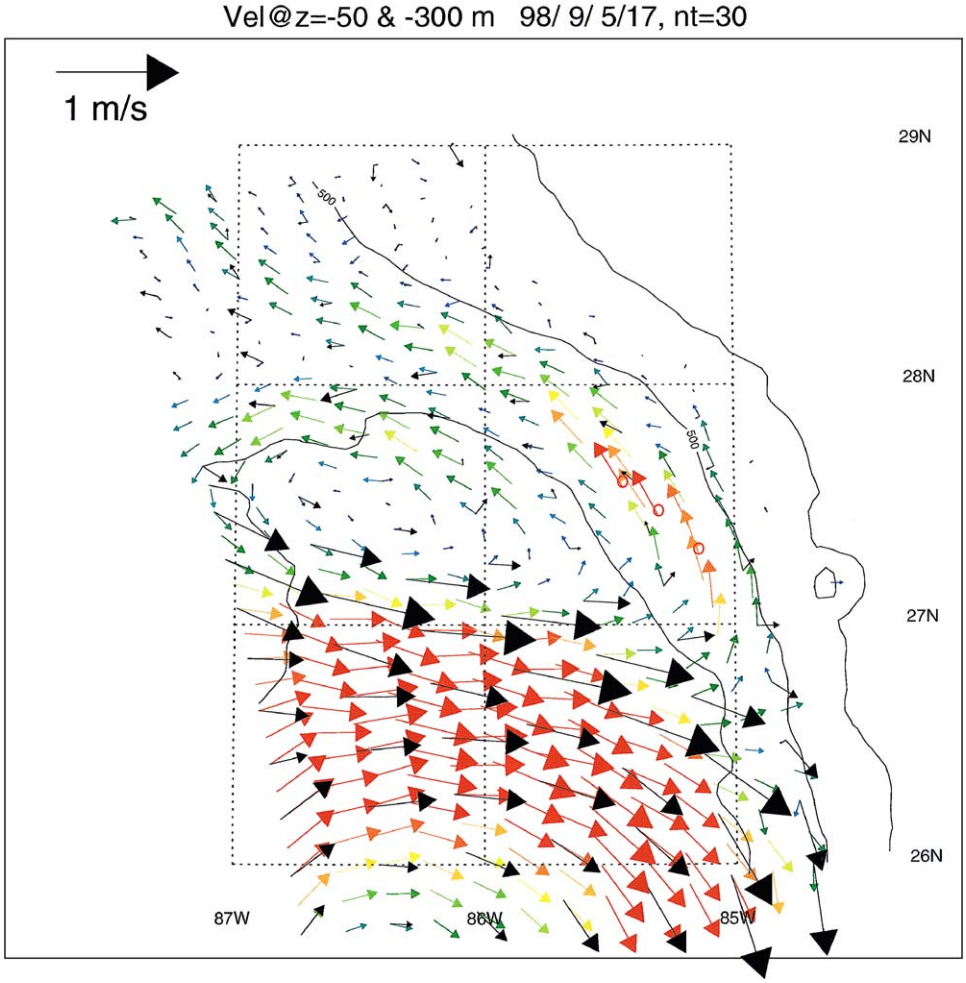

Fig. 15. Simulated velocity vectors at $z = -50$ m (black) and $z = -300$ m (colors: red $> 0.45\,\mathrm{m\,s^{-1}}$ and blue $< 0.05\,\mathrm{m\,s^{-1}}$) on Sep/5/1998) over the west Florida slope. The subsurface jet and mixing front are indicated by red circles. Contours are 200, 500 and 3000 m isobaths.

(e.g. parallel with MPIs, nesting). Also, the availability of higher-resolution (and timely) observations (ADCP, CODAR, satellite, floats, etc) will enable us to examine more critically the circulation physics and also to evaluate models. Typical depths at the shelf-edge and slope range from 100 to 3000 m. Thus fine-grid sizes $\approx$ depths, and the scale-overlap implies that, *for some processes*, we might question the validity of a hydrostatic model (POM is one). The relaxation of the hydrostatic constraint should be a priority in the near future. Non-hydrostatic general circulation models have emerged in recent years (e.g. Marshall et al., 1997). They should be more widely tested; the shelf-edge and slope seem to be an ideal test site. Finally, realistic modeling (rather than idealized process studies) that includes both open-ocean (e.g. slope current, large eddies, winds, tides) and near-coast (e.g. river plumes, shelf currents, wind and waves, tides) influences, together with data assimilation and concomitant model/data analyses, will be quite an exciting challenge (cf. Wang et al., 2003).

Acknowledgements

This work was supported by the Minerals Management Service and the Office of Naval Research. Shejun Fan helped with the graphics. We thank two anonymous reviewers for their useful comments. Computing was done at GFDL/NOAA, Princeton.

References

Brown, O.B., Cornillon, P.C., Emmerson, S.R., Carle, H.M., 1986. Gulf Stream warm rings: a statistical study of their behavior. Deep-Sea Research 33 (11–12A), 1459–1473.

Cheney, R.E., Richardson, P.L., 1976. Observed decay of cyclonic Gulf Stream rings. Deep-Sea Research 23 (2), 143–155.

Cochrane, J.D., 1972. In: Capurro, L.R.A., Reid, J.L. (Eds.), Separation of an Anticyclone and Subsequent developments in the Loop Current (1969), Vol 2. Texas A & M Univ. Ocean Studies, Gulf Publishing Co., Houston, pp. 91–106.

Davies, A.M., Xing, J., 2000. Modelling of turbulent mixing at the shelf edge. Continental Shelf Research 20 (14), 1789–1823.

Dewar, W.K., Killworth, P.D., Blundell, J.R., 1999. Primitive-equation instability of wide oceanic rings, Part II, numerical studies of ring stability. Journal of physical Oceanography 29, 1744–1758.

Ezer, T., Oey, L.-Y., Sturges, W., Lee, H.-C., 2003. The variability of currents in the Yucatan Channel: analysis of results from a numerical ocean model. Journal of Geophysical Research 10.1029/2002JC001509.

Fratantoni, D.M., Johns, W.E., Townsend, T.L., 1995. Rings of the North Brazil Current: their structure and behavior inferred from observations and a numerical simulation. Journal of Geophysical Research 100, 10633–10654.

Fratantoni, P.S., Lee, T.N., Podesta, G.P., Muller-Karger, F., 1998. The influence of Loop Current perturbations on the formation and evolution of Tortugas eddies in the southern Strait of Florida. Journal of Geophysical Research 103, 24759–24799.

Gill, A.E., 1982. Atmosphere–Ocean Dynamics. Academic Press, New York 662pp.

Grimshaw, R., Broutman, D., He, X., Sun, P., 1994. Analytical and numerical study of a barotropic eddy on a topographic slope. Journal of physical Oceanography 24, 1587–1607.

Hamilton, P., Fargion, G.S., Biggs, D.C., 1999. Loop Current eddy paths in the western Gulf of Mexico. Journal of physical Oceanography 29, 1180–1207.

Hamilton, P., Berger, T.J., Johnson, W., 2002. On the structure and motions of cyclones in the northern Gulf of Mexico. Journal of Geophysical Research 1073208, doi:10.1029, 1–18.

Haney, R.L., 1991. On the pressure gradient force over steep topography in sigma coordinate ocean models. Journal of physical Oceanography 21, 610–619.

Kirwan Jr., A.D., Lewis, J.K., Indest, A.W., Reinersman, P., Quintero, I., 1988. Observed and Simulated Kinematic Properties of Loop Current Rings. Journal of Geophysical Research 93, 1189–1198.

Kurihara, Y., Bender, M.A., 1980. Use of a movable nested-mesh model for tracking a small vortex. Monthly Weather Review 108, 1792–1809.

LaCasce, J.H., 1998. A geostrophic vortex over a slope. Journal of physical Oceanography 28, 2362–2381.

Lewis, J.K., Kirwan Jr., A.D., 1985. Some observations of ring topography and ring-ring interactions in the Gulf of Mexico. Journal of Geophysical Research 90, 9017–9028.

Marshall, J., Hill, C., Perelman, L., Adcroft, A., 1997. Hydrostatic, quasi-hydrostatic, and nonhydrostatic ocean modeling. Journal of Geophysical Research Oceans, 102 (C3), 5733–5752.

Matsuura, T., Yamagata, T., 1982. On the evolution of nonlinear planetary eddies larger than the radius of deformation. Journal of physical Oceanography 12, 440–456.

Mellor, G.L., Yamada, T., 1982. Development of a turbulence closure model for geophysical fluid problems. Review of Geophysical and Space Physics 20, 851–875.

Mellor, G.L., Blumberg, A.F., 1985. Modeling vertical and horizontal diffusivities with the sigma coordinate system. Monthly Weather Review 113, 1380–1383.

Mellor, G.L., 1991. An equation of state for numerical models of oceans and estuaries. Journal of Atmospheric Oceanic Technology 8, 609–611.

Mellor, G.L., Oey, L.-Y., Ezer, T., 1998. Sigma coordinate pressure gradient errors and the seamount problem. Journal of Atmospheric Oceanic Technology 15, 1122–1131.

Mellor, G.L., 2002. User guide for a three-dimensional, primitive equation, numerical ocean model (Jul/2002 version), 42pp., Prog. in atmos. and Oceanic Sci., Princeton University, 2002. [See http://www.aos.princeton.edu/WWWPUBLIC/htdocs.pom/PubOnLine/POL.html].

Nof, D., 1999. Strange encounters of eddies with walls. Journal of Marine Research 57, 739–761.

Oey, L.-Y., 1995. Eddy- and wind-forced shelf circulation. Journal of Geophysical Research 100, 8621–8637.

Oey, L.-Y., 1996a. Simulation of mesoscale variability in the Gulf of Mexico. Journal of physical Oceanography 26, 145–175.

Oey, L.-Y., 1996b. The accuracy of a nested-grid ocean model. Princeton University Atmospheric & Oceanic Sci. Report#1996-03, pp.28, 25 figures.

Oey, L.-Y., 1998. Eddy energetics in the Faroe-Shetland Channel. Continental Shelf Research 17, 1929–1944.

Oey, L.-Y., Chen, P., 1992a. A model simulation of circulation in the north-east Atlantic shelves and seas. Journal of Geophysical Research 97, 20087–20115.

Oey, L.-Y., Chen, P., 1992b. A nested-grid simulation of the Norwegian coastal current. Journal of Geophysical Research 97, 20063–20086.

Oey, L.-Y., Lee, H.-C., 2002. Deep eddy energy and topographic Rossby waves in the Gulf of Mexico. Journal of physical Oceanography 32, 3499–3527.

Oey, L.-Y., Lee, H.-C., SchmitzJr., W.J., 2003a. Effects of Winds and Caribbean Eddies on the Frequency of Loop Current Eddy Shedding: A Numerical Model Study. Journal of Geophysical Oceanography 108 (C10), 3324, doi:10.1029/2002JC001698.

Oey, L.-Y., Hamilton, P., Lee, H.-C., 2003b. Modeling and Data-Analyses of Circulation Processes in the Gulf of Mexico. Final Report to the Minerals Management Service, Contract#1435-01-99-CT-31028; 116pp, 56 figures. Available from Science Applications International Corporation, 615 Oberlin Rd., Suite 100, Raleigh, NC 27605.

Oey, L.-Y., Fan, S.-J., Lee, H.-C., 2003c. Model Descriptions of Subsurface Jets in the Gulf of Mexico. Princeton University Atmospheric & Oceanic Sci. Report#2003–01, pp.25, 11 figures.

Richardson, P.L., Hufford, G.E., Limeburner, R., 1994. North Brazil Current retroflection eddies. Journal of Geophysical Research 99, 5081–5093.

Schlichting, H., 1968. Boundary Layer Theory. McGraw-Hill, New York 748 pp.

Schmitz Jr., W.J., 1996. On the World Ocean Circulation: Vol. I—Some Global Features/North Atlantic Circulation. WHOI Technical Report WHOI-96-03, 141 pp.

Shi, C., Nof, D., 1993. The splitting of eddies along boundaries. Journal of Marine Research 51, 771–795.

Smagorinsky, J., 1963. General circulation experiments with the primitive equations Part I: the basic experiment. Monthly Weather Review 91, 99–164.

Smith IV, D.C., 1986. A numerical study of Loop Current eddy interaction with topography in the western Gulf of Mexico. Journal of physical Oceanography 16, 1260–1272.

Smith IV, D.C., Bird, A.A., 1989. Factors influencing asymmetry and self advection in ocean eddies. In: Nihoul, J.C.J., Jamart, B.M. (Eds.), Mesoscale/Synoptic Coherent Structures in Geophysical Turbulence. Elsvier Science Pub., Amsterdam, pp. 211–224.

Smith IV, D.C., O'Brien, J.J., 1983. The interaction of a two-layer isolated mesoscale eddy with topography. Journal of physical Oceanography 13, 1681–1697.

Sutyrin, G.G., Rowe, G.D., Rothstein, L.M., Ginis, I., 2003. Baroclinic eddy interactions with continental slope and shelves. Journal of physical Oceanography 33, 283–291.

Teague, W.J., Carron, M.J., Hogan, P.J., 1990. A comparison between the Generalized Digital Environmental Model and Levitus climatologies. Journal of Geophysical Research 95, 7167–7183.

Vidal, V.M.V., Vidal, F.V., Perez-Molero, J.M., 1992. Collision of a Loop Current anticyclonic ring against the continental slope of the western Gulf of Mexico. Journal of Geophysical Research 97, 2155–2172.

Vukovich, F.M., Maul, G.A., 1985. Cyclonic eddies in the eastern Gulf of Mexico. Journal of physical Oceanography 15, 105–117.

Vukovich, F.M., Waddel, E., 1991. Interaction of a warm ring with the western slope in the Gulf of Mexico. Journal of physical Oceanography 21, 1062–1074.

Wang, D.P., 1993. Model of frontogenesis: subduction and upwelling. Journal of Marine Research 51, 497–513.

Wang, D.-P., Oey, L.-Y., Ezer, T., Hamilton, P., 2003. Nearsurface currents in DeSoto Canyon. Journal of physical Oceanography 33, 313–326.

Zavala-Sanson, L., Graef, F., Pavia, E.G., 1998. Collision of anticyclonic, lens-like eddies with a meridional western boundary. Journal of Geophysical Research 103, 24881–24890.